Submitted to Physical Review B

FSU-SCRI-98-81
CU-NPL-1162

arXiv:cond-mat/9808310v1 [cond-mat.str-el] 27 Aug 1998

Mean-Field Theory for Spin Ladders Using Angular-Momentum Coupled Bases

J. Piekarewicz
Department of Physics and Supercomputer Computations Research Institute, Florida State University, Tallahassee, FL 32306

J.R. Shepard
Department of Physics, University of Colorado, Boulder, CO 80309

(February 1, 2008)

Abstract

We study properties of two-leg Heisenberg spin ladders in a mean-field approximation using a variety of angular-momentum coupled bases. The mean-field theory proposed by Gopalan, Rice, and Sigrist, which uses a rung basis, assumes that the mean-field ground state consists of a condensate of spin-singlets along the rungs of the ladder. We generalize this approach to larger angular-momentum coupled bases which incorporate—by their mere definition—a substantial fraction of the important short-range structure of these materials. In these bases the mean-field ground-state remains a condensate of spin singlet—but now with each involving a larger fraction of the spins in the ladder. As expected, the "purity" of the ground-state, as judged by the condensate fraction, increases with the size of the elementary block defining the basis. Moreover, the coupling to quasiparticle excitations becomes weaker as the size of the elementary block increases. Thus, the weak-coupling limit of the theory becomes an accurate representation of the underlying mean-field dynamics. We illustrate the method by computing static and dynamic properties of two-leg ladders in the various angular-momentum coupled bases.

I. INTRODUCTION

Spin ladders have received much recent attention due to their likely relevance to high-T_c superconductors. The full arsenal of theoretical many-body physics methods has been brought to bear on the problem of spin ladders, including direct diagonalization (DD) [1], Lanczos techniques [2], quantum Monte Carlo (QMC) [1], density matrix renormalization

group (DMRG) [3], high-order perturbation theory augmented by re-summation techniques [4], mappings to effective field theories [5,6] as well as quasi-analytic methods based on mean-field approaches [7]. In the present work, we focus on the last of these techniques and extend the mean-field theory (MFT) of Gopalan, Rice and Sigrist [7]. This extension includes a derivation of generalized mean-field equations appropriate to any angular-momentum coupled basis. In particular, we examine MFT's utilizing bases whose elements are eigenstates of 2×1 ("rung"basis), 2×2 ("plaquette" basis) and 2×4 systems. The original work of Ref. [7] employed a rung basis. Indeed, the strong coupling limit for which coupling within rungs is much greater than coupling between rungs—in which case the ladder ground state can be well-approximated by a configuration in which every rung is coupled to a spin singlet—was the inspiration for their MFT in which rung singlets "condense". We also do MFT calculations in the rung basis but obtain rather different results from those of Ref. [7]. The likely origin of these differences is addressed below. We find our rung-basis MFT results in much better agreement with known properties of 2-leg ladder—such as the ground state energy per site, the spin gap, the spin correlation length [3], the one-magnon dispersion relation [8], and the strength of the $S(\pi,\pi)$ spin response [9]—than those of Ref. [7]. Our results suggest that rung-basis MFT is a relatively simple but still robust means of accounting for the physics of spin ladders.

We also study plaquette- and 2×4-basis MFTs. In a previous work [10], we showed that the plaquette basis offers some significant advantages over simpler bases (including the rung basis) when describing the physically relevant [11] case of isotropic spin ladders where intra-rung and inter-rung couplings are equal. We find here that the plaquette basis yields an MFT which is superior to that of the rung basis. While the two sets of calculations give very similar mean-field values for many ladder observables, we conclude that only the plaquette basis results are reliable. This determination is based on the fact that our estimates of contributions beyond mean-field theory are quite large for the rung basis but much smaller for plaquettes. As our general approach holds for any angular-momentum coupled basis, we also study the MFT utilizing a 2×4 basis. Here, MFT results are comparable to those for the rung and plaquette MFTs. We trace the lack of significant improvement upon going to this rather complicated basis to truncations which become increasingly severe as the basis is built from the eigenstates of larger and larger systems. In this context, the plaquette basis MFT seems the best compromise between building enough physics into the basis that MFT can account for the bulk of the physics and, at the same time, avoiding severe truncations.

The paper is organized as follows: In Section II, we present our angular-momentum coupled formalism for spin ladders in the context of the rung basis. We also present our rung-basis MFT and identify differences with Ref. [7]. In addition, we derive weak-coupling expansions for the energy per site and spin gap which are useful in understanding the physics embodied in the MFT equations (and which additionally reproduce the full MFT results with surprising accuracy, especially for the plaquette basis). We next indicate how to make a perturbative estimate of corrections to the energy per site and spin gap arising from terms in the Hamiltonian which are omitted at the mean-field level. Finally we extend our MFT to plaquette and 2×4 bases and indicate where and with what justification truncations are made. Numerical results and discussion of them appear in Section III, while Section IV contains our conclusions.

II. FORMALISM

A. Two-leg Ladder Hamiltonian

The Heisenberg Hamiltonian for a two-leg ladder with nearest-neighbor antiferromagnetic coupling is given by

$$H = J_{\parallel} \sum_{\leftrightarrow} \mathbf{S}_i \cdot \mathbf{S}_j + J_{\perp} \sum_{\updownarrow} \mathbf{S}_i \cdot \mathbf{S}_j \ . \tag{1}$$

Here $J_{\perp}$ and $J_{\parallel}$ are the strength of the antiferromagnetic coupling along the rungs and chains of the ladder, respectively [1]. In the strong-coupling limit, $\lambda \equiv \ J_{\parallel}/J_{\perp} \rightarrow 0$, the interaction between rungs is very weak and the above separation of the Hamiltonian is, indeed, a natural one. In this limit the Hamiltonian can be separated into a large component H_0, which contains the strong intra-rung interactions, and a weak "two-body" potential V between rungs. That is, $H = H_0 + \lambda V$, where

$$H_0 = \sum_{r=1}^{N} \mathbf{S}_1(r) \cdot \mathbf{S}_2(r) \ , \tag{2}$$

$$V = \sum_{r=1}^{N} \left[\mathbf{S}_1(r) \cdot \mathbf{S}_1(r+1) + \mathbf{S}_2(r) \cdot \mathbf{S}_2(r+1) \right] \ . \tag{3}$$

Note that we have set $J_{\perp} \equiv 1$ and that r labels a specific rung in the N-rung ladder. Further, $\mathbf{S}_1(r)[\mathbf{S}_2(r)]$ denotes the spin operator for the electron on the first[second] site of the r-th rung. The rung basis is particularly suitable in the strong-coupling regime, as H_0 is diagonal in this basis. The eigenvalues and eigenvectors of H_0 are of the form:

$$|\phi_{\ell m}\rangle = |(s_1 s_2)\, \ell m\rangle \ ; \quad \epsilon_{\ell} = \frac{1}{2}\ell(\ell+1) - 3/4 \ . \tag{4}$$

Here the two spins along a definite rung in the ladder are coupled to a total angular momentum ℓ, which can be zero or one, and projection m. Rung singlet and triplet creation operators are defined accordingly

$$A^{\dagger}_{\ell m}(r) \equiv \left[c^{\dagger}_1(r) \otimes c^{\dagger}_2(r) \right]_{\ell m} \ , \tag{5}$$

where $c^{\dagger}$ is an electron creation operator. Note that the rung singlet/triplet operators satisfy the usual commutation relations for bosons:

$$[A_{\ell m}(r), A^{\dagger}_{\ell' m'}(r')] = \delta_{\ell \ell'} \delta_{m m'} \delta_{r r'} \ . \tag{6}$$

We now proceed to rewrite the above Hamiltonian in a second-quantized form. For the unperturbed part of the Hamiltonian, namely, the part that is diagonal in the rung basis, we obtain

$$H_0 = \sum_{r=1}^{N} \sum_{\ell=0}^{1} \hat{\ell} \epsilon_{\ell} \left[A^{\dagger}_{\ell}(r) \otimes \widetilde{A}_{\ell}(r) \right]_{0,0} = \sum_{r=1}^{N} \left[\epsilon_0 s^{\dagger}(r) s(r) - \epsilon_1 \mathbf{t}^{\dagger}(r) \cdot \widetilde{\mathbf{t}}(\mathbf{r}) \right] \ , \tag{7}$$

where we have defined $\hat{\ell} \equiv \sqrt{2\ell+1}$ and

$$s^\dagger(r) \equiv A^\dagger_{00}(r) \; ; \quad t^\dagger_m(r) \equiv A^\dagger_{1m}(r) \; . \tag{8}$$

Note that we have also introduced the "tilde" operators through the definition:

$$\widetilde{t}_m = (-1)^{1-m} t_{-m} \; . \tag{9}$$

As we have indicated explicitly in Eq. (7) it is the operator $\widetilde{\mathbf{t}}$—not $\mathbf{t}$—that transforms as a vector under rotations; the m-dependent phase factor in the above equation is necessary to enforce this condition. In analogy to the one-body term, the two-body potential energy [Eq. (3)] can be written in a rotationally-invariant form

$$V = \sum_{r=1}^{N} \sum_{\ell'_1 \ell'_2 \ell_1 \ell_2 j} \hat{\jmath} \, \langle \ell'_1 \ell'_2 j || V(1,2) || \ell_1 \ell_2 j \rangle \left[\Big(A^\dagger_{\ell'_1}(r) A^\dagger_{\ell'_2}(r+1) \Big)_j \Big(\widetilde{A}_{\ell_1}(r) \widetilde{A}_{\ell_2}(r+1) \Big)_j \right]_{00} \; . \tag{10}$$

Matrix elements of the potential have been computed in Ref. [8] and have been listed—along with the corresponding matrix elements in other bases—in Table I. It is important to mention that due to the symmetry of the potential only two of these matrix elements are independent. We have chosen them to be:

$$\alpha \equiv \langle 011 || V(1,2) || 101 \rangle \quad \text{and} \quad \beta \equiv \langle 110 || V(1,2) || 110 \rangle \; . \tag{11}$$

If we now assume periodic boundary conditions, then the total linear momentum becomes also a good quantum number. Thus, it is convenient to re-write the Hamiltonian in momentum space. To this end, we start by performing a Fourier transformation of the spin singlet and triplet operators

$$A^\dagger_{\ell m}(r) = \frac{1}{\sqrt{N}} \sum_k e^{ikr} A^\dagger_{\ell m}(k) \; ; \qquad \left(k = \frac{2\pi\nu}{N} \; ; \;\; \nu = 1, 2, \ldots, N \right) \; . \tag{12}$$

Moreover, we decomposed the Hamiltonian into three components:

$$H = H_0 + \lambda H_1 + \lambda H_2 \; . \tag{13}$$

The first term in this decomposition is simply the unperturbed Hamiltonian of Eq. (7) written in momentum space

$$H_0 = \sum_k \Big[\epsilon_0 s^\dagger(k) s(k) - \epsilon_1 \mathbf{t}^\dagger(k) \cdot \widetilde{\mathbf{t}}(k) \Big] \; . \tag{14}$$

The second term represents that part of the two-body potential that is bilinear in both the spin-singlet and spin-triplet operators. It is given by

$$H_1 = \frac{1}{N} \sum_{k_1 k_2 q} \alpha \cos(q) \Big[\mathbf{t}^\dagger(k'_1) \cdot \mathbf{t}^\dagger(k'_2) s(k_2) s(k_1) - \mathbf{t}^\dagger(k'_1) \cdot \widetilde{\mathbf{t}}(k_2) s^\dagger(k'_2) s(k_1) + \text{h.c.} \Big] \; . \tag{15}$$

Note that we have introduced the two "final" momenta by defining $k'_1 \equiv k_1 - q$ and $k'_2 \equiv k_2 + q$. Finally, H_2 is the remaining—quartic in the spin-triplet operator—part of the potential:

$$H_2 = \frac{1}{N}\sum_{j=0}^{2}\sum_{k_1 k_2 q} C_j \beta \cos(q) \left[\Big(\mathbf{t}^\dagger(k_1') \mathbf{t}^\dagger(k_2') \Big)_j \Big(\widetilde{\mathbf{t}}(k_2) \widetilde{\mathbf{t}}(k_1) \Big)_j \right]_{00} , \tag{16}$$

where $C_j \equiv (-1)^{j+1} \hat{\jmath}\, (1-3\delta_{j0})/2$. Note that there is no component of the potential having an odd number of spin-triplet operators because of the selection rule $\ell_1 + \ell_2 + \ell_1' + \ell_2' =$ even [8].

We now conclude this section by introducing the "grand-canonical" Hamiltonian K through the definition

$$K = H - \mu N \, . \tag{17}$$

Here μ is the chemical potential and N is the number operator given by

$$N = \sum_k \Big[s^\dagger(k) s(k) + \sum_m \mathbf{t}_m^\dagger(k) \mathbf{t}_m(k) \Big] = \sum_k \Big[s^\dagger(k) s(k) - \mathbf{t}^\dagger(k) \cdot \widetilde{\mathbf{t}}(k) \Big] \, . \tag{18}$$

As long as no approximations are being made, the description of the interacting system in term of either H or K is equally acceptable. The virtue of K, however, is in that it allows a consistent treatment of the system even if the "particle" number is not conserved (i.e., if $[H, N] \neq 0$). Since the mean-field approximation of the next chapter is based on a Bogoliubov transformation, using the grand-canonical Hamiltonian K provides a definite advantage over H.

B. Mean-Field Approximation

In this section we implement the mean-field approximation of Gopalan, Rice, and Sigrist [7]. The central dynamical assumption of their model is that the spin-singlet bosons with zero linear momentum form a condensate. Hence, it becomes natural to replace the spin-singlet operators by "c-numbers", i.e.,

$$s(k), s^\dagger(k) \longrightarrow \sqrt{N} \bar{s}\, \delta_{k,0} \, . \tag{19}$$

If this condition is now substituted on the above expressions for H_0 and H_1 [Eqs. (14,15), respectively] we obtain

$$H_0 = N \bar{s}^2 \epsilon_0 - \epsilon_1 \sum_k \mathbf{t}^\dagger(k) \cdot \widetilde{\mathbf{t}}(k) \, , \tag{20a}$$

$$H_1 = \bar{s}^2 \sum_k \alpha \cos(k) \Big[\mathbf{t}^\dagger(k) \cdot \mathbf{t}^\dagger(-k) - \mathbf{t}^\dagger(k) \cdot \widetilde{\mathbf{t}}(k) + \text{h.c.} \Big] \, . \tag{20b}$$

These expressions are now bilinear in the spin-triplet operators and, thus, amenable for diagonalization via a Bogoliubov transformation. Note that H_2 [Eq. (16)] remains quartic in the spin-triplet operators. Hence, for the moment we will ignore this term in the determination of the mean-field ground state and will return to it later to compute its effect perturbatively. In this way, the mean-field Hamiltonian can be written in the following compact form

$$K_{\text{MF}}(\bar{s}^2, \mu) = N(\epsilon_0 - \mu)\bar{s}^2 - \frac{3}{2} N(\epsilon_1 - \mu) + \frac{1}{2} \sum_{km} \mathcal{T}_m^\dagger(k)\, \Omega(k)\, \mathcal{T}_m(k) \, . \tag{21}$$

where

$$\mathcal{T}_m(k) = \begin{bmatrix} \mathbf{t}_m(+k) \\ \\ \widetilde{\mathbf{t}}^{\dagger}_m(-k) \end{bmatrix} \quad \text{and} \quad \Omega(k) = \begin{pmatrix} \Lambda(k) & -2\Delta(k) \\ -2\Delta(k) & \Lambda(k) \end{pmatrix} . \tag{22}$$

Note that the two independent elements of the 2×2 matrix $\Omega(k)$ are given by

$$\Lambda(k) = \epsilon_1 - \mu + 2\lambda\alpha\bar{s}^2\cos(k) \quad \text{and} \quad \Delta(k) = \lambda\alpha\bar{s}^2\cos(k) . \tag{23}$$

The above mean-field Hamiltonian can now be diagonalized by means of a standard Bogoliubov transformation. We obtain

$$K_{\rm MF}(\bar{s}^2,\mu) = N(\epsilon_0-\mu)\bar{s}^2 - \frac{3}{2}N(\epsilon_1-\mu) + \frac{3}{2}\sum_k \omega(k) + \sum_{km}\omega(k)\gamma^{\dagger}_m(k)\gamma_m(k) , \tag{24}$$

where

$$\omega(k) = \sqrt{\Lambda(k)^2 - 4\Delta^2(k)} = (\epsilon_1-\mu)\sqrt{1+d\cos(k)} \; ; \quad \Big(d \equiv 4\lambda\alpha\bar{s}^2/(\epsilon_1-\mu)\Big) . \tag{25}$$

Moreover, the new "quasiparticle" creation operators are defined by

$$\gamma^{\dagger}_m(k) = u(k)\mathbf{t}^{\dagger}_m(k) - v(k)\widetilde{\mathbf{t}}_m(-k) , \tag{26}$$

where the coefficients generating the canonical transformation—satisfying $[u^2(k)-v^2(k)]=1$—are given by

$$u(k) = \sqrt{\frac{\Lambda(k)+\omega(k)}{2\omega(k)}} \quad \text{and} \quad v(k) = \text{sgn}[\Delta(k)]\sqrt{\frac{\Lambda(k)-\omega(k)}{2\omega(k)}} . \tag{27}$$

The mean-field ground state—the quasiparticle vacuum—is now determined by the condition

$$\gamma_m(k)|\Phi_0\rangle = 0 , \quad \text{for all } k \text{ and } m . \tag{28}$$

As we have described in the appendix, we have carried out the Bogoliubov transformation by diagonalizing an appropriate 2×2 random-phase-approximation (RPA) matrix. Although not explicitly treated in the appendix, the method has the virtue of being easily generalizable to matrices of arbitrary dimension. We should mention that for the particular case of the rung basis (i.e., $\epsilon_0=-3/4$, $\epsilon_1=1/4$, and $\alpha=1/2$) our results are identical to those obtained in Ref. [7]—with one exception. The two factors of 3/2 appearing in Eq. (24) appear as factors of 1/2 in Ref. [7]. In our derivation these factors arise from the zero-point motion of the three triplet "oscillators", one for every magnetic component of $\mathbf{t}$. We will examine the quantitative impact of this difference in Sec. III.

Ground-state observables can now be obtained by taking appropriate derivatives of the thermodynamic potential

$$K_0(\bar{s}^2,\mu) \equiv \langle\Phi_0|K_{\rm MF}(\bar{s}^2,\mu)|\Phi_0\rangle = N(\epsilon_0-\mu)\bar{s}^2 - \frac{3}{2}N(\epsilon_1-\mu) + \frac{3}{2}\sum_k \omega(k) . \tag{29}$$

For example, the number of rungs can be recovered by using the thermodynamic relation

$$N = -\left(\frac{\partial K_0(\bar{s}^2,\mu)}{\partial \mu}\right) \ , \tag{30}$$

or equivalently, from the following transcendental equation

$$\bar{s}^2 - \frac{5}{2} + \frac{3}{2}\Big[\mathcal{I}(d) - d\mathcal{I}'(d)\Big] = 0 \ ; \quad \mathcal{I}(d) \equiv \int_0^{2\pi} \frac{dk}{2\pi}\sqrt{1+d\cos(k)} \ . \tag{31}$$

This equation serves to write d—and, thus, the chemical potential μ—in terms of $\bar{s}^2$. Note that the function $d(\bar{s}^2)$ is "universal"; it is independent of the value of the ratio of $J_\parallel$ to $J_\perp$ and of the choice of basis. Finally, the expectation value of the singlet condensate may be determined from minimizing the ground-state energy with respect to $\bar{s}^2$

$$\left(\frac{\partial E_0(\bar{s}^2)}{\partial \bar{s}^2}\right) = 0 \ ; \quad E_0(\bar{s}^2) \equiv K_0(\bar{s}^2,\mu(\bar{s}^2)) + \mu(\bar{s}^2)N \ . \tag{32}$$

Having determined the values of the chemical potential μ and the singlet condensate $\bar{s}^2$, static observables—such as the energy-per-site and the one-magnon dispersion relation $\omega(k)$—can be easily computed.

C. Dynamic Spin Response

Perhaps more exciting is the possibility of computing the dynamic spin response of the system. This kind of computation has proven to be particularly challenging in certain approaches—such as DMRG—as transition matrix elements, in addition to the excitation spectrum, must be computed. Yet the dynamic response constitutes one of the most fundamental properties of the system and one that may soon be extracted from new data on inelastic neutron scattering experiments from single crystals.

For two leg-ladders one can define two independent spin responses, $S_0(q,\omega)$ and $S_\pi(q,\omega)$, according to the relative phase between the two spin operators along the rungs of the ladder. That is,

$$S_{0,\pi}(q,\omega) = \sum_n \Big|\langle\Psi_n|S_{0,\pi}(q)|\Psi_0\rangle\Big|^2 \delta(\omega-\omega_n) \ , \tag{33}$$

where Ψ_0 is the exact ground-state wavefunction of the system, Ψ_n an excited state with excitation energy ω_n, and the transition operator is given by

$$S_{0,\pi}(q) = \sum_r e^{iqr}\Big[\mathbf{S}_1(r) \pm \mathbf{S}_2(r)\Big]_z \ . \tag{34}$$

Although similar in form, these two operators probe very different aspects of the dynamics of the system. This can be seen most easily by expressing both transition operators in a second-quantized form:

$$\Big[\mathbf{S}_1(r) + \mathbf{S}_2(r)\Big]_m = \sqrt{2}\Big[\mathbf{t}^\dagger(r)\otimes\tilde{\mathbf{t}}(r)\Big]_{1m} \ ; \tag{35a}$$

$$\Big[\mathbf{S}_1(r) - \mathbf{S}_2(r)\Big]_m = \Big[\mathbf{t}^\dagger_m(r)s(r) - s^\dagger(r)\tilde{\mathbf{t}}_m(r)\Big] \underset{\text{MF}}{\longrightarrow} \bar{s}\Big[\mathbf{t}^\dagger_m(r) - \tilde{\mathbf{t}}_m(r)\Big] \ . \tag{35b}$$

These equations imply that S_π probes the low-energy part of the spectrum, as it couples the ground-state of the system to the one-magnon band. In contrast, S_0—a two-magnon operator—probes the high-energy part of the response. Thus, the S_π response becomes instrumental in elucidating the important low-energy/low-temperature behavior of the system.

Matrix elements of the above operators can be readily evaluated by expressing the spin-triplet operators in terms of the quasiparticle operators of Eq. (26). We obtain

$$\frac{1}{N}S_0(q,\omega) = 2\int_0^{2\pi}\frac{dk}{2\pi}\Big[u(k)v(k+q) - u(k+q)v(k)\Big]^2\delta\Big(\omega - \omega(k) - \omega(k+q)\Big)\;; \tag{36a}$$

$$\frac{1}{N}S_\pi(q,\omega) = \bar{s}^2\Big[u(q) - v(q)\Big]^2\delta\Big(\omega - \omega(q)\Big) = \frac{\bar{s}^2}{\sqrt{1+d\cos(q)}}\,\delta\Big(\omega - \omega(q)\Big)\;. \tag{36b}$$

Note that, given q and ω, the delta function in Eq. (36a) constrains the integral over k with the result that not only is the S_0 response pushed to high-energy but, in addition, it is strongly fragmented. This is in contrast to the S_π response that is predicted to be concentrated in a single excitation at $\omega = \omega(q)$. At least for the $S_\pi(q=\pi,\omega)$ response, this is in good agreement with an earlier calculation [9] on a 2×16 ladder that predicts almost 95 percent of the strength to be concentrated at an excitation energy equal to the singlet-triplet gap. Finally, having computed the two dynamic response functions the spin-spin correlation function per site can be easily extracted:

$$\langle\Phi_0|S_z(0)S_z(r)|\Phi_0\rangle = \frac{1}{8}\int_0^{2\pi}\frac{dq}{2\pi}e^{iqr}\Big[S_0(q) + S_\pi(q)\Big]/N\;, \tag{37}$$

where the static structure factors have been defined by

$$S_{0,\pi}(q) = \int_0^\infty d\omega\, S_{0,\pi}(q,\omega)\;. \tag{38}$$

Note that in Eq. (37) both spins are located on the same chain of the ladder at a distance of r rungs. As we will see shortly the long-range behavior of the spin-spin correlation function is dominated by the static structure factor $S_\pi(q)$, namely,

$$\langle\Phi_0|S_z(0)S_z(r)|\Phi_0\rangle \approx \frac{1}{8}\int_0^{2\pi}\frac{dq}{2\pi}e^{iqr}S_\pi(q)/N = \frac{\bar{s}^2}{8}\int_0^{2\pi}\frac{dq}{2\pi}\frac{e^{iqr}}{\sqrt{1+d\cos(q)}}\;. \tag{39}$$

We can see that, in the spirit of the stationary-phase approximation, the principal contribution to the integral at large r occurs where the rapid oscillation of the exponential factor is canceled by rapid changes in $[1+d\cos(q)]^{-1/2}$. This will happen near any of the singularities of the latter factor. Indeed, upon using the steepest-descent technique we obtain the expected exponential behavior of the spin-spin correlation function and our analytic approximation for the correlation length:

$$\langle\Phi_0|S_z(0)S_z(r)|\Phi_0\rangle \sim e^{-r/\xi}\;;\quad \xi = 1/\ln\Big[d/(1-\sqrt{1-d^2})\Big]\,. \tag{40}$$

D. Weak-Coupling Expansions

To gain further insight into the mean-field theory of Ref. [7] we derive in this section weak-coupling ($\lambda \ll 1$) expansions for various observables. We start this procedure with an expansion of Eq. (31), which determines the parameter d—or equivalently the chemical potential—in terms of the parameter $\bar{t}^2 \equiv 1 - \bar{s}^2$. That is,

$$\left(\frac{d^2}{16}\right) + \frac{45}{4}\left(\frac{d^2}{16}\right)^2 + \mathcal{O}(d^6) = \frac{2}{3}\bar{t}^2 \;\longrightarrow\; \left(\frac{d^2}{16}\right) = \frac{2}{3}\bar{t}^2 - 5\bar{t}^4 + \mathcal{O}(t^6)\;. \tag{41}$$

This equation can now be substituted into the ground-state energy to yield an expression that is correct to fourth-order in the small parameter $\bar{t} = \mathcal{O}(\lambda)$:

$$E_0(\bar{t}) = \epsilon_0 - \delta\bar{t} + \Delta_0\bar{t}^2 - \frac{\delta}{4}\bar{t}^3 + \mathcal{O}(\bar{t}^5)\;; \quad \text{where } \delta \equiv \sqrt{6}\lambda|\alpha|\;. \tag{42}$$

By minimizing the above expression for the energy with respect to $\bar{t}$, ground-state—and even some excited-state—observables can be determined. Indeed, from the minimization procedure the singlet condensate is readily obtained

$$\bar{s}^2 = 1 - \frac{3}{2}\left(\frac{\lambda\alpha}{\Delta_0}\right)^2\left[1 + \frac{9}{4}\left(\frac{\lambda\alpha}{\Delta_0}\right)^2 + \mathcal{O}(\lambda^4)\right]\;. \tag{43}$$

Moreover, having determined the behavior of the singlet condensate in terms of λ, one can generate—through Eqs. (25) and (41)—the corresponding behavior of the chemical potential. This is all that is required to compute the mean-field observables. For example, we obtain the following perturbative expansions for the ground-state energy per rung and for the singlet-triplet gap, respectively:

$$E_0 = \epsilon_0 - \frac{3}{2}\frac{(\lambda\alpha)^2}{\Delta_0}\left[1 + \frac{3}{4}\left(\frac{\lambda\alpha}{\Delta_0}\right)^2 + \mathcal{O}(\lambda^4)\right]\;, \tag{44a}$$

$$\Delta = \Delta_0 - 2\lambda|\alpha|\left[1 - \frac{1}{2}\left(\frac{\lambda|\alpha|}{\Delta_0}\right) + \frac{1}{2}\left(\frac{\lambda|\alpha|}{\Delta_0}\right)^2 + \mathcal{O}(\lambda^3)\right]\;. \tag{44b}$$

Note that the small parameter in the above expansions is given by $\lambda\alpha/\Delta_0$.

E. Perturbative Contribution From H_2

An important assumption of the mean-field approximation of Ref. [7] is that H_2—the term of the Hamiltonian quartic in the spin-triplet operators [Eq. (16)]—changes the mean-field results only slightly. To test the validity of this assumption we now estimate the effect of H_2 on the ground-state energy and on the one-magnon dispersion relation using first-order perturbation theory.

The first-order correction to the ground-state energy due to H_2 is given by

$$\Delta E_0 = \lambda\langle\Phi_0|H_2|\Phi_0\rangle\;. \tag{45}$$

To evaluate this correction to the energy the four spin-triplet operators in H_2 [Eq. (16)] are expanded in terms of the quasiparticle operators—$\gamma_m(k)$ and $\gamma_m^\dagger(k)$—and the resulting matrix elements are evaluated using Wick's theorem. We obtain,

$$\Delta E_0/N = 3\lambda\beta\left[\Big(\int_0^{2\pi}\frac{dk}{2\pi}u(k)\cos(k)v(k)\Big)^2-\Big(\int_0^{2\pi}\frac{dk}{2\pi}v(k)\cos(k)v(k)\Big)^2\right]. \tag{46}$$

Note that only those combinations of quasiparticle operators that conserved quasiparticle number need to be considered. The corresponding perturbative contribution to the one-magnon band is slightly more complicated to evaluate. Still, it can be efficiently computed from the following double-commutator formula:

$$\Delta\omega(k) = \lambda\Big[\langle\Phi_0|\gamma_m(k)\,H_2\,\gamma_m^\dagger(k)|\Phi_0\rangle - \langle\Phi_0|H_2|\Phi_0\rangle\Big] = \lambda\langle\Phi_0|\Big[\gamma_m(k),[H_2,\gamma_m^\dagger(k)]\Big]|\Phi_0\rangle\,. \tag{47}$$

In this way the resulting expression for the first-order correction to the dispersion relation becomes

$$\begin{aligned}\Delta\omega(k) = 2\lambda\beta\Bigg(&2u(k)v(k)\cos(k)\int_0^{2\pi}\frac{dq}{2\pi}u(q)\cos(q)v(q)\\&-\Big[u^2(k)+v^2(k)\Big]\cos(k)\int_0^{2\pi}\frac{dq}{2\pi}v(q)\cos(q)v(q)\Bigg).\end{aligned} \tag{48}$$

F. Mean-Field Theory with Improved Bases

The mean-field theory of the previous section is fully characterized by three parameters: the spin-singlet energy ϵ_0, the spin-triplet energy ϵ_1, and the singlet-triplet matrix element α (if corrections to the mean-field observables need to be computed, an additional triplet-triplet matrix element, β, is necessary). This suggests that the generalization of the mean-field method of Gopalan, Rice, and Sigrist [7] to larger angular-momentum coupled bases is straightforward. Moreover, the advantage of the larger bases is that they incorporate part of the short-range structure of the system—and, thus, an important part of the physics—exactly.

One such basis is the "plaquette" basis introduced by us in Ref. [10]. The plaquette basis is generated from coupling the four spins in a 2×2 lattice. Specifically, the two diagonal pairs of spins are coupled to well-defined total angular momenta, ℓ_{14} and ℓ_{23}, which can equal zero or one. These two "link" angular momenta are in turn coupled to a total plaquette angular momentum j and projection m. The physically appealing feature of the plaquette basis is that the 2×2 ladder Hamiltonian with isotropic ($J_\parallel = J_\perp \equiv 1$) coupling is diagonal in the plaquette basis. That is

$$H(2\times 2)\Big|\ell_{14}\ell_{23},jm\Big\rangle = \frac{1}{2}\Big[j(j+1)-\ell_{14}(\ell_{14}+1)-\ell_{23}(\ell_{23}+1)\Big]\Big|\ell_{14}\ell_{23},jm\Big\rangle\,. \tag{49}$$

The lowest spin-singlet ($j=0$) eigenstate arise from coupling the two link angular momenta to their maximum value of $\ell_{14}=\ell_{23}=1$. The corresponding value for the energy is given by $\epsilon_0=-2$. Next comes the three-fold degenerate spin-triplet ($\ell_{14}=\ell_{23}=j=1$) eigenstate

with an energy of $\epsilon_1 = -1$. Note that these four states—out of a total of sixteen—define the low-energy basis the we have used earlier in a study of the dynamic spin response [9]. It is precisely these four low-energy states that we retain here to generalize the mean-field theory of Ref. [7] to the plaquette basis. The sole remaining parameter needed to define the mean-field theory is the singlet-triplet matrix element α. In the plaquette basis it is given by $\alpha = -1/3$. It is interesting to note that the ratio of α to the unperturbed gap Δ_0—which is a measure of the "goodness" of the basis [see Eq. (44)]—improves as one goes from the rung to the plaquette basis: $|\alpha/\Delta_0|$ goes from 1/2 to 1/3.

We can also compute the two dynamic spin responses in the plaquette basis. Indeed, the S_0 and S_π operators of Eq. (34) can be re-expressed in terms of the four spin operators along a 2×2 plaquette. We obtain

$$S_0(q) = e^{-iq/2} \sum_p e^{i2qp} \Big[\cos(q/2) \Big(\mathbf{S}_1(p) + \mathbf{S}_2(p) + \mathbf{S}_3(p) + \mathbf{S}_4(p) \Big)_z - i \sin(q/2) \Big(\mathbf{S}_1(p) + \mathbf{S}_2(p) - \mathbf{S}_3(p) - \mathbf{S}_4(p) \Big)_z \Big] \; ; \tag{50a}$$

$$S_\pi(q) = e^{-iq/2} \sum_p e^{i2qp} \Big[\cos(q/2) \Big(\mathbf{S}_1(p) - \mathbf{S}_2(p) + \mathbf{S}_3(p) - \mathbf{S}_4(p) \Big)_z - i \sin(q/2) \Big(\mathbf{S}_1(p) - \mathbf{S}_2(p) - \mathbf{S}_3(p) + \mathbf{S}_4(p) \Big)_z \Big] \; . \tag{50b}$$

Note that $\mathbf{S}_1(p)[\mathbf{S}_3(p)]$ and $\mathbf{S}_2(p)[\mathbf{S}_4(p)]$ denote the first and second spin operators along the first[second] rung of the p-th plaquette. Moreover, the sum over p now runs over all plaquettes in the ladder and the Fourier sum includes $2q$—not q—as the variable conjugate to p. In spite of their apparent complexity the above expressions are identical to the ones given in Eq. (34). The virtue of writing them in such a form becomes evident as one takes their mean-field limit. Indeed, in this limit the dynamic spin responses take the following simple form:

$$\frac{1}{N} S_0(q,\omega) = 0 \; ; \tag{51a}$$

$$\frac{1}{N} S_\pi(q,\omega) = \frac{8}{3} \bar{s}^2 \frac{\sin^2(q/2)}{\sqrt{1 + d\cos(2q)}} \, \delta\Big(\omega - \omega(2q)\Big) \; . \tag{51b}$$

Perhaps more than anything else these expressions capture the essence of the mean-field approximation in the plaquette basis. Clearly, the S_0 response is not zero [see. Eq. (36a)]. Yet, it is small and its strength is fragmented and located at very high excitation energy. The "low-energy" plaquette basis—the truncated basis obtained by retaining only the lowest spin-singlet and spin-triplet states—can not account for the physics at high excitation energy. In contrast the S_π response, which couples the ground-state to the one-magnon band, probes the low-excitation part of the spectrum and should be well described using the low-energy plaquette basis.

One could continue to systematically improve the basis. For example, the spectrum of isotropic 2×4 and 2×8 ladders have been previously calculated in Ref. [9]. In particular, the lowest singlet and triplet energies of the 2×4 ladder (with open boundary conditions) are

given by $\epsilon_0 = -4.29307$ and $\epsilon_1 = -3.52286$, respectively. Moreover, from the 2×8 calculation the singlet-triplet matrix element can also be extracted; it is given by: $\alpha = -0.20805 \simeq -1/5$. Thus, the mean-field theory can be further extended to the 2×4 basis. Note that for this basis $|\alpha/\Delta_0| \sim 1/4$. Although one has obtained a better expansion parameter in this basis relative to the plaquette basis, the improvement has been somewhat reduced by the fact that as the singlet-triplet matrix element α goes down so does the unperturbed gap. Moreover, the truncation errors increase considerably; while one retains the same four states in both bases, the dimension of the vector space goes from 16 in the plaquette basis to 256 in the 2×4 basis. This will become an important issue in our final analysis. Values for the mean-field parameters in the various bases are tabulated in Table I.

III. RESULTS

In this section we report mean-field results for the energy-per-site, the singlet-triplet gap, the one-magnon dispersion relation, the spin-spin correlation function, and the dynamic spin response using various angular-momentum coupled bases. Because of the nature of these bases, any comparison among them will only be carried out at the isotropic ($\lambda = 1$) point.

A. Rung Basis

We start with a presentation of our results in the rung basis. In Table II we have listed the ground-state energy-per-site for three values of λ. The second column contains the mean-field numbers reported in Ref. [7], while the third column contains the corresponding values as obtained by us. The difference between these values originates solely from the treatment of the zero-point motion; recall that a factor of 1/2, rather than 3/2, was used in Ref. [7]. While the impact of this error on the spin gap has been discussed recently in Ref. [12], we feel compelled to address it here as well, as the mean-field theory of Gopalan, Rice, and Sigrist seems to work much better for most observables—not only for the spin gap—than their original results might suggest. Indeed, even for the most unfavorable case of $\lambda = 1$, the corrected mean-field results are within 6 percent—not 18 percent—of the exact answer. Fig. 1 presents these results in graphical form and serves as a further testimony to this fact.

For the spin gap the improvement is even more dramatic. In Table II and Fig. 2 we display results for the singlet-triplet gap (in units of $J_\perp$) as a function of λ. The filled circles in the figure (labeled "exact") were obtained from a very high-order perturbative expansion [4] supplemented by a Padé analysis. This plot shows conclusively that the mean-field theory of Ref. [7] captures an important part of the physics governing the ladder materials. While the perfect agreement at the isotropic point seems a bit fortuitous, it is clear that the mean-field theory provides—in addition to an intuitive physical picture—a very robust starting point for more sophisticated calculations.

In Fig. 3 we show our mean-field results for the spin-triplet dispersion band (in units of $J_\perp$) relative to the value at the band minimum $\Delta = \omega(\pi)$. The filled circles for $\lambda = 0.1$ and 0.5 are the result of a perturbative calculation [8], while those at $\lambda = 1$ were obtained from

the fit to Lanczos results carried out in Ref. [13]. We observe that for $\lambda \leq 0.5$ the agreement with exact results is relatively good even for the states at the top of the one-magnon band.

We now proceed to discuss the two dynamic spin responses. In Fig. 4 we display our results for $S_0(q,\omega)$ and for $S_\pi(q,\omega)$ as a function of the excitation energy ω for various values of the momentum transfer q. For clarity, all of the S_0 responses have been multiplied by a factor of ten, while the S_π responses include an artificial smearing of the delta function:

$$\delta(\omega-\omega_0) \approx \frac{\eta/\pi}{(\omega-\omega_0)^2+\eta^2} \; ; \quad \eta = 0.02 \; . \tag{52}$$

As suggested in our earlier discussion the S_0 response is indeed small and—as it probes the two-magnon structure of the system—it is located at high-excitation energy and its strength is strongly fragmented. In contrast, the S_π response is concentrated in a single excitation and, at least for $q \simeq \pi$, it is located at low-excitation energy ($\omega \gtrsim \Delta$). The fact that all the S_π strength is concentrated in one fragment suggests that, once the dispersion band is computed [see. Fig. 3], all that remains to fully characterize the $S_\pi(q,\omega)$ response is to determine the static structure factor $S_\pi(q)$. Such a plot is displayed in Fig. 5 where $S_0(q)$ also appears. The figure clearly shows that $S_0(q)$ is not only appreciably smaller than $S_\pi(q)$ but it is also considerably smoother. This suggests that the large Fourier components of the sum of the two structure factors—and thus the long-range behavior of the spin-spin correlation function—will, indeed, be dominated by $S_\pi(q)$. Thus, Eq. (40) can be used to estimate the spin-spin correlation length:

$$\xi \approx \frac{1}{\ln\left[d/(1-\sqrt{1-d^2})\right]} \underrightarrow{d=0.914} = 2.323 \; . \tag{53}$$

Note that a value of $\xi = 2.211$ for the correlation length, extracted from an exponential fit to the full numerical evaluation of the spin-spin correlation function, compares well with the simple analytic estimate given above—but differs substantially from the exact value of $\xi = 3.19$ [3].

B. Extension to Larger Bases

In this section we compare mean-field results obtained on a variety of angular-momentum coupled bases. We have alluded earlier to the fact that for gapped systems with a relatively small correlation length—such as the two-leg ladder materials studied here—incorporating as much as possible of the short-distance structure of the system into the definition of the basis is clearly advantageous [9,14]. The three angular-momentum coupled bases considered here are defined as the eigenstates of the $2 \times L$ Heisenberg ladder, with $L = 1$, 2, and 4; for $L = 1$ and 2 these are the rung and plaquette basis, respectively. For simplicity—and because of their intrinsic interest—we limit ourselves to the physically relevant case of isotropic ($J_\perp = J_\parallel \equiv 1$) ladders.

In Table III we list results for the ground-state energy-per-site and for the single-triplet gap in various approximations; the next to last column contains the exact—basis-independent—results obtained from the DMRG calculation of Ref. [3], while the last column lists the spin-singlet condensate fraction. This last column makes evident that the "purity"

of the ground-state increases as one incorporates more and more of the short-range structure of the system. However, as severe truncations must be made, the overall picture does not necessarily improve with the size of the basis. The second column contains the zeroth-order results. These results are obtained from the mere definition of the basis and are independent of any approximation. We observe that for these gapped systems incorporating as much as possible of the short-range dynamics into the definition of the basis is, indeed, advantageous. For example, for the 2×4 basis the zeroth-order result for the energy is already within seven percent of the exact answer. For the gap—a much more sensitive quantity—the result still differs from the exact answer by 50 percent. Yet, this is significantly better than the factor-of-two discrepancy obtained in the rung and plaquette bases. The third column lists the mean-field results. We observe that for the energy-per-site the reduction relative to the zeroth-order values is in good agreement with the second-order estimate from Eq. (44a). That is,

$$[\Delta E_0/\text{site}]_{\text{MF}} \simeq \begin{cases} -0.18750 & \text{for the } 2\times 1 \text{ basis;} \\ -0.04167 & \text{for the } 2\times 2 \text{ basis;} \\ -0.01054 & \text{for the } 2\times 4 \text{ basis.} \end{cases} \tag{54}$$

It is interesting to note that although the zeroth-order estimate for the energy-per-site varies substantially among the three bases (up to 30 percent) the mean-field approximation brings all of them to within one percent of each other—and to within approximately five percent of the exact answer. In the fourth column we have included the first-order correction coming from H_2 (see Sec.II E):

$$[\Delta E_0/\text{site}]_{H_2} = \begin{cases} -0.04564 & \text{for the } 2\times 1 \text{ basis;} \\ -0.00386 & \text{for the } 2\times 2 \text{ basis;} \\ -0.00050 & \text{for the } 2\times 4 \text{ basis.} \end{cases} \tag{55}$$

In all cases the correction to the energy-per-site is small relative to the mean-field contribution, and justifies—albeit *a posteriori*—treating H_2 perturbatively.

The situation changes dramatically, however, upon examination of the singlet-triplet gap. In contrast to the energy-per-site which has a lowest-order contribution proportional to λ^2, the mean-field contribution to the spin gap starts with the term $-2\lambda|\alpha|$. Although, for $\lambda = 1$, the correction from the higher-order terms is not negligible, this linear term dominates. Note that while the mean-field correction to the spin gap is close to 40 percent in the 2×4 basis, the corresponding correction to the energy-per-site is a meager 2 percent. Moreover, it is now no longer justifiable—specifically in the case of the rung basis—to treat H_2 perturbatively. Indeed, the almost-perfect agreement between the rung-basis mean-field and the exact answer is lost. While, on its own, this result does not invalidate the mean-field approach, a careful re-assessment of the role of H_2 is clearly necessary.

The impact of H_2 on the gap, however, seems to be more moderate for the larger bases. For example, there is only a ten and three percent correction to the gap in the plaquette and 2×4 basis, respectively. This seems to indicate that the whole approach, namely, mean-field plus H_2, is under control for these larger bases. Yet the agreement with the exact result in the particular case of the 2×4 basis is poor (of the order of 15 percent). We attribute this behavior to the severe truncation of the basis; recall that in the 2×4 basis only four out of a total of 256 states have been retained.

Overall, it seems that the plaquette basis offers the best compromise. While there are non trivial perturbative corrections to the gap from H_2, these are moderate—unlike the corrections computed in the rung basis. Moreover, while we do truncate the basis, the truncation errors are not as severe as in the 2×4 basis. This is reflected in the "bracketing" of the exact result for the gap between the mean-field and the mean-field plus H_2 estimates. Further, because of the "small" expansion parameter in the plaquette basis [$(\lambda\alpha/\Delta_0)^2 = \lambda^2/9$] most of the mean-field behavior can be reproduced with terms up to order λ^2 in the perturbative expansion. This is illustrated in Fig. 6 where we have plotted the ground-state energy-per-site and the spin gap as a function of λ. The filled circles, essentially an exact calculation, are from a previous perturbative estimate [8]. Note that the $\lambda \neq 1$ case represents a pair of dimerized chains connected to each other by transverse bonds of strength equal to one of the two intra-chain couplings. To the best of our knowledge, a physical realization of this "dimerized ladder" is yet to be found. Yet, as it is well known, the isotropic limit of these ladders has been the object of intense scrutiny [11].

We conclude this section with a discussion of plaquette-basis results for the dynamic spin response $S_\pi(q,\omega)$; recall that in a mean-field approximation with the low-energy (truncated) plaquette basis the $S_0(q,\omega)$ response is identically zero. As the strength of the S_π response is concentrated in a single excitation, it is sufficient to present results for the one-magnon dispersion band and for the static structure factor in order to fully characterize its behavior. Thus, in Fig. 7 we display the dispersion relation for the one-magnon band at the isotropic value. The solid and dashed lines (practically indistinguishable in the figure) represent the mean-field and the mean-field plus H_2 results, respectively. The filled circles were computed from a a fit to Lanczos data [13]. We observe that the plaquette results describe accurately the high-momentum/low-energy part of the band, but deteriorate rapidly as one moves to the low-momentum/high-energy region. This behavior is to be expected, as the discarded (high-energy) states in the plaquette basis account for most of the high-energy properties of the systems. In the near future we are planning to incorporate additional high-energy states into the mean-field model in order to improve the description of the high-energy properties of the system. Fortunately, as is evident in Fig. 8 [see also Fig. 5], the discarded high-energy states are of little consequence to the dynamic spin response, which has most of its strength concentrated at low excitation energy. Moreover, this is the region that controls the long-range behavior of the spin-spin correlation function, which is shown in the inset on Fig. 8. According to Eq. (51), the plaquette-basis spin-spin correlation function per site is then given by

$$\langle \Phi_0 | S_z(0) S_z(r) | \Phi_0 \rangle = \frac{\bar{s}^2}{6} \int_0^{2\pi} \frac{dq}{2\pi}\, e^{iqr}\, \frac{\sin^2(q/2)}{\sqrt{1+d\cos(2q)}}\,. \tag{56}$$

A steepest-descent evaluation of the integral on the rhs of this equation yields, in analogy with Eq. (40) for the rung basis,

$$\langle \Phi_0 | S_z(0) S_z(r) | \Phi_0 \rangle \simeq e^{-r/\xi}\,; \quad \xi = 2/\ln\left[-d/(1-\sqrt{1-d^2})\right] \tag{57}$$

where we must recall that, in the plaquette basis, $d<0$, while d is positive in the rung basis. A fit to the full result for the correlation function (see Fig. (8)) gives a value of $\xi = 3.098$ for the correlation length, which is within seven percent of the approximate analytic value of

$$\xi \approx \frac{2}{\ln\left[-d/(1-\sqrt{1-d^2})\right]} \overset{d=-0.843}{\longrightarrow} = 3.327. \tag{58}$$

These results compare very well—at the three-percent level—with the exact value of $\xi = 3.19$ obtained from the DMRG analysis of Ref. [3]. Our results for correlation lengths using both rung and plaquette bases are summarized in Table IV.

IV. CONCLUSIONS

We have computed magnetic properties of Heisenberg spin-1/2 ladders using an extension of the mean-field approximation of Gopalan, Rice, and Sigrist [7] which we have implemented using a variety of angular-momentum coupled bases. In the original version of the model—which employed the rung basis exclusively—the Heisenberg Hamiltonian was written in terms of spin-singlet and spin-triplet operators. Because of the rotational symmetry of the Hamiltonian, the full theory is specified in terms of only four parameters; these are the rung-singlet and rung-triplet energies, and two off-diagonal matrix elements. In the limit in which the ratio (λ) of the coupling of the spins along the chains of the ladder relative to the coupling along the rungs is negligible, the ground-state wavefunction becomes a direct product of spin-singlets on every rung of the ladder. The first spin excitation is reached by breaking a spin-singlet along any of the rungs of the ladder. This weak-coupling limit of the theory is the motivation behind the mean-field approximation of Ref. [7]. Hence, in this approximation, one assumes that the spin-singlet bosons of zero linear momentum are condensed. This enables one to separate the Heisenberg Hamiltonian into a part that is quadratic in the spin-triplet operators $\mathbf{t}$—the mean-field Hamiltonian—and a part (H_2) that remains quartic in $\mathbf{t}$. The mean-field Hamiltonian is then brought to a diagonal form by means of a Bogoliubov transformation while the quartic part must be treated by some other means.

As the mean-field Hamiltonian is determined by only a small number of parameters, its generalization to larger bases is straightforward. The physical motivation behind the change of basis is the small value (of the order of three lattice sites) of the spin-spin correlation length. Thus, the main advantage of the larger bases is that they can incorporate exactly—by their mere definition—part of the important short-range dynamics of these gapped systems.

Our first calculations were carried out in the rung basis, as in Ref. [7]. We implemented the mean-field procedure through a Bogoliubov transformation, which although standard, was effected here via a diagonalization of a suitable RPA-like matrix. One of the virtues of such an approach is that the generalization to larger vector spaces becomes simple. This is of special interest to us, as our future mean-field work will incorporate additional high-energy states of the plaquette basis. Our rung-basis results differ from those presented by the authors of Ref. [7] due to what we believe was an oversight on their part. Our results indicate that, contrary to their first reports, their mean-field approach works well at a quantitative level. Indeed, we find that the results for the energy-per-site and for the singlet-triplet gap agree with exact calculations to within six percent all through the $0 \leq \lambda \leq 1$ range (note, however, that the value for the spin-spin correlation length at the isotropic point was heavily underestimated: $\xi = 2.211 < 3.19$). In particular, the spin gap differs from the exact answer by less than one percent at the isotropic point. Unfortunately, this nice agreement was lost

once the contribution from H_2 was estimated perturbatively. Incorporating the effects from H_2 in a reliable manner should constitute an important goal for future work.

For the larger 2×2 (plaquette) and 2×4 bases considered here an additional approximation was required. We assumed that the important physics of the spin-ladder materials is dominated by the lowest singlet and triplet states in the corresponding bases; note that it is only in the rung basis that the singlet and triplet states are unique. We found that while rung- and plaquette-basis results are of similar quality for most ladder observables, only the latter ones were stable upon including the perturbative contribution from H_2. This is a direct consequence of the size of the elementary block defining the basis. As the larger bases incorporate more of the short-range dynamics of the system, the quartic piece of the Hamiltonian (H_2) decreases in importance as the size of the elementary block increases. Since our general approach is easily extended to any angular-momentum coupled basis, mean-field studies were also carried out utilizing a 2×4 basis. The results obtained with this basis did not improve—and in some cases worsen—the agreement relative to the plaquette basis. We have traced this behavior to the severe truncations made in the 2×4 basis; only four out of a total of 256 states were retained. Thus, we conclude that the plaquette basis offers the best compromise between building enough short-range physics into the definition of the basis, while avoiding too severe a truncation. Indeed, plaquette-basis mean-field results for the energy-per-site, the spin gap, and the spin-spin correlation function are within five percent of the quoted DMRG values [3].

In the future, we plan to complete a number of extensions of the mean-field treatment. For example, we have truncated the spectrum of spin triplet states in the plaquette basis retaining only those of lowest energy. Although we have observed that this is a good approximation for describing the low-energy dynamics, it is not adequate to describe the high-energy properties. This requires an extension of the usual Bogoliubov technique for bringing quadratic Hamiltonians involving a single species of field operator into diagonal form. We have already made considerable progress in this direction and we are planning to publish our results in the near future. Alternatively, one could still retain the truncated basis but account for the truncation errors through a suitable renormalization of the matrix elements. Indeed, one such technique—CORE, or the contractor renormalization group method [15]—has been used successfully by us in computing static and dynamic properties of up to 2×16 ladders [9]. Such an approach, to be used in the near future, could also be valuable in the context of the mean-field theory. We are also planning to develop a version of the mean-field theory for ladders which treats the quartic terms of the Hamiltonian self-consistently, rather than just perturbatively as it was done here. Finally—and of special relevance to the high-T_c materials—we are planning to use the mean-field theory in the various angular-momentum coupled bases to study the physics of lightly-doped ladders [16].

APPENDIX: BOGOLIUBOV TRANSFORMATION

In this appendix we carry out the Bogoliubov transformation via a diagonalization of a random-phase-approximation (RPA) matrix. In order to do so we write the—operator part—of the mean-field Hamiltonian of Eq. (21) in matrix form. That is,

$$\hat{K}_{\rm MF}(\bar{s}^2,\mu) \equiv \frac{1}{2}\sum_{km} \mathcal{T}^\dagger_m(k)\,\Omega(k)\,\mathcal{T}_m(k)\ . \tag{A1}$$

Although we illustrate the method using the 2×2 matrix of Eq. (22) the method can be easily generalized to matrices of arbitrary dimension.

Given that the matrix $\Omega(k)$ is symmetric, it can be diagonalized via a similarity transformation. The problem with such an approach, however, is that the resulting orthogonal matrix generates a new set of creation and annihilation operators that are not consistent with each other. Instead, what is required is to write Eq. (A1) in terms of a matrix having an RPA-like structure, i.e.,

$$\hat{K}_{\rm MF}(\bar{s}^2,\mu) = \frac{1}{2}\sum_{km} \mathcal{T}^\dagger_m(k)\,g\,\Omega_{\rm RPA}(k)\,\mathcal{T}_m(k)\ , \tag{A2}$$

where we have introduced the "metric" $g \equiv {\rm diag}\{1,-1\}$ and have defined $\Omega_{\rm RPA} \equiv g\Omega$. We now list, without proof, some useful properties of RPA matrices:

1. Eigenvalues of $\Omega_{\rm RPA}$ come in pairs; if ω is an eigenvalue of $\Omega_{\rm RPA}$ so is $-\omega$.

2. Eigenvectors of $\Omega_{\rm RPA}$ corresponding to different eigenvalues are orthonormal with respect to the metric g: $\langle\omega'|g|\omega\rangle = {\rm sgn}(\omega)\,\delta_{\omega'\omega}$.

3. There exists a "similarity" transformation $\mathcal{S}$—with its columns being the eigenvectors of $\Omega_{\rm RPA}$—that brings $\Omega_{\rm RPA}$ into a diagonal form: $\mathcal{S}^{-1}\,\Omega_{\rm RPA}\,\mathcal{S} = {\rm diag}\{\omega,-\omega\}$, where $\mathcal{S}^{-1} = g\,\mathcal{S}^T g$.

Using these properties, and defining a new set of creation and annihilation operators through $\Gamma_m \equiv \mathcal{S}^{-1}\mathcal{T}_m$, the mean-field Hamiltonian becomes explicitly diagonal. That is,

$$\hat{K}_{\rm MF}(\bar{s}^2,\mu) = \frac{1}{2}\sum_{km} \Gamma^\dagger_m(k)\begin{pmatrix}\omega(k) & 0\\ 0 & \omega(k)\end{pmatrix}\Gamma_m(k) = \frac{3}{2}\sum_k \omega(k) + \sum_{km}\omega(k)\gamma^\dagger_m(k)\gamma_m(k)\ . \tag{A3}$$

APPENDIX: ACKNOWLEDGMENTS

This work was supported by the DOE under Contracts Nos. DE-FC05-85ER250000, DE-FG05-92ER40750 and DE-FG03-93ER40774.

REFERENCES

[1] T. Barnes, E. Dagotto, J. Riera and E.S. Swanson, Phys. Rev. **B47**, 3196 (1993).
[2] E. Dagotto, Rev. Mod. Phys. **66**, 763 (1994).
[3] S.R. White, R.M. Noack and D.J. Scalapino, Phys. Rev. Lett. **73**, 886 (1994).
[4] Zheng Weihong, V. Kotov and J. Oitmaa, `cond-mat/9711006`.
[5] Mattias Troyer, Hirokazu Tsunetsugu and T.M. Rice, `cond-mat/9510150`.
[6] D.G. Shelton, A.A. Nerseyan and A.M. Tsvelik, Phys. Rev. **B53**, 8521 (1996).
[7] Sudha Gopalan, T.M. Rice and M. Sigrist, Phys. Rev. **B49**, 8901 (1994).
[8] J. Piekarewicz and J.R. Shepard, Phys. Rev. **B**, in press; `cond-mat/9804261`.
[9] J. Piekarewicz and J.R. Shepard, Phys. Rev. **B57**, 10260 (1998).
[10] J. Piekarewicz and J.R. Shepard, Phys. Rev. **B56**, 5366 (1997).
[11] E. Dagotto and T.M. Rice, Science **271**, 618 (1996).
[12] B. Normand and T.M. Rice, Phys. Rev. **B54**, 7180 (1996); we are grateful to Prof. Rice for pointing out this reference to us.
[13] T. Barnes and J. Riera, Phys. Rev. **B50**, 6817 (1994).
[14] E. Dagotto, G. B. Martins, J. Riera, A. L. Malvezzi, and C. Gazza, `cond-mat/9707205`.
[15] C.J. Morningstar and M. Weinstein, Phys. Rev. Lett. **73**, 1873 (1994); Phys. Rev. D**54**, 4131 (1996).
[16] M. Sigrist, T.M. Rice and F.C. Zhang, Phys. Rev. **B49**, 12058 (1994).

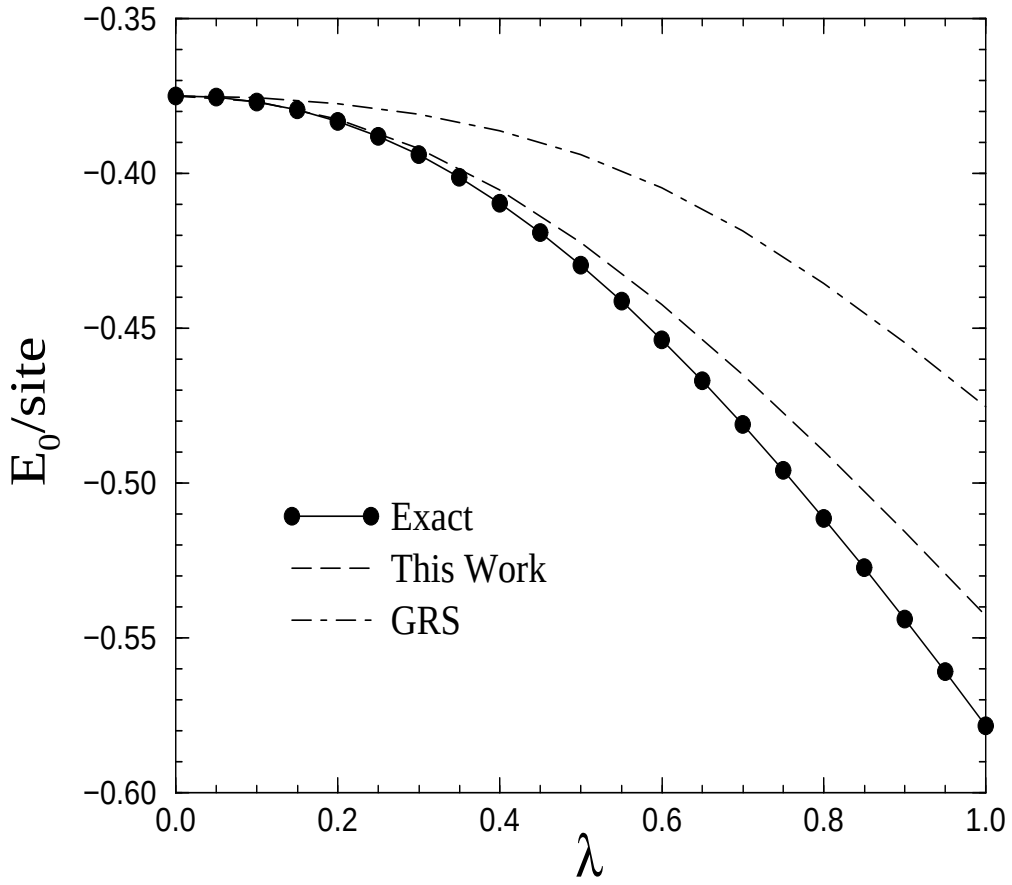

FIG. 1. Ground-state energy-per-site (in units of $J_\perp$) as a function of λ. The filled circles are "exact" results obtained from a very high-order perturbative expansion [4], while GRS are the results of Gopalan, Rice, and Sigrist [7].

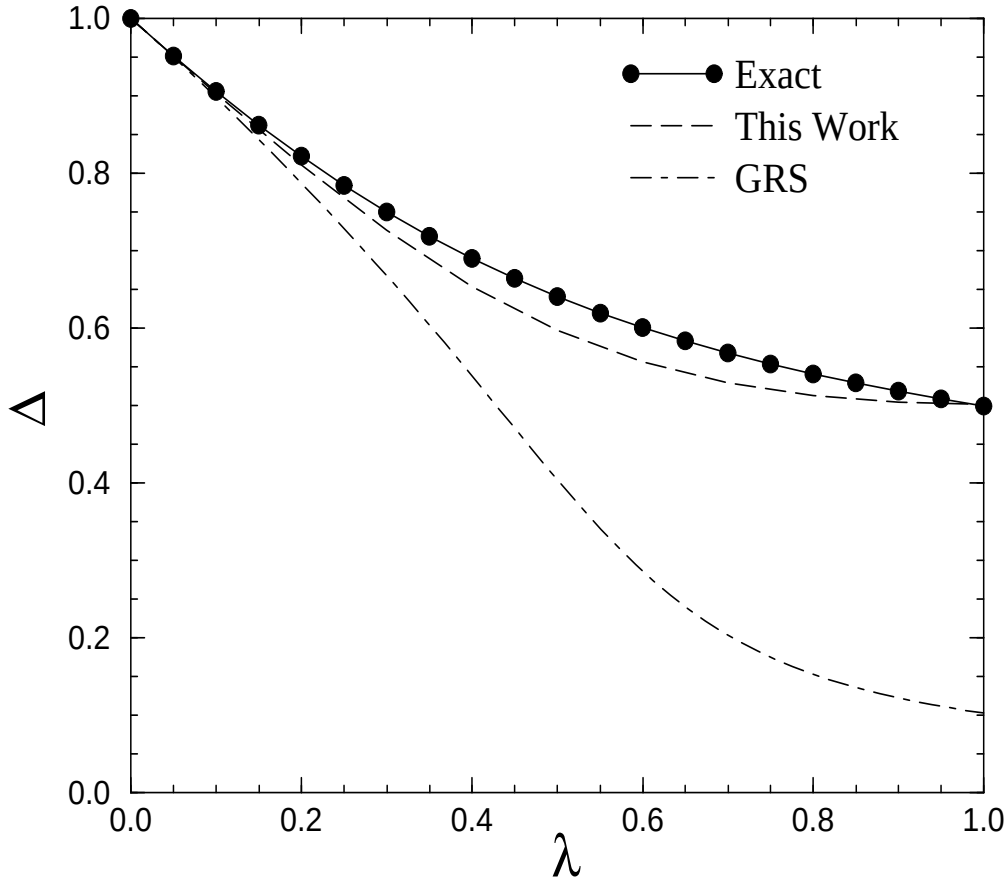

FIG. 2. Singlet-triplet gap (in units of $J_\perp$) as a function of λ. The filled circles are "exact" results obtained from a very high-order perturbative expansion [4], while GRS are the results of Gopalan, Rice, and Sigrist [7].

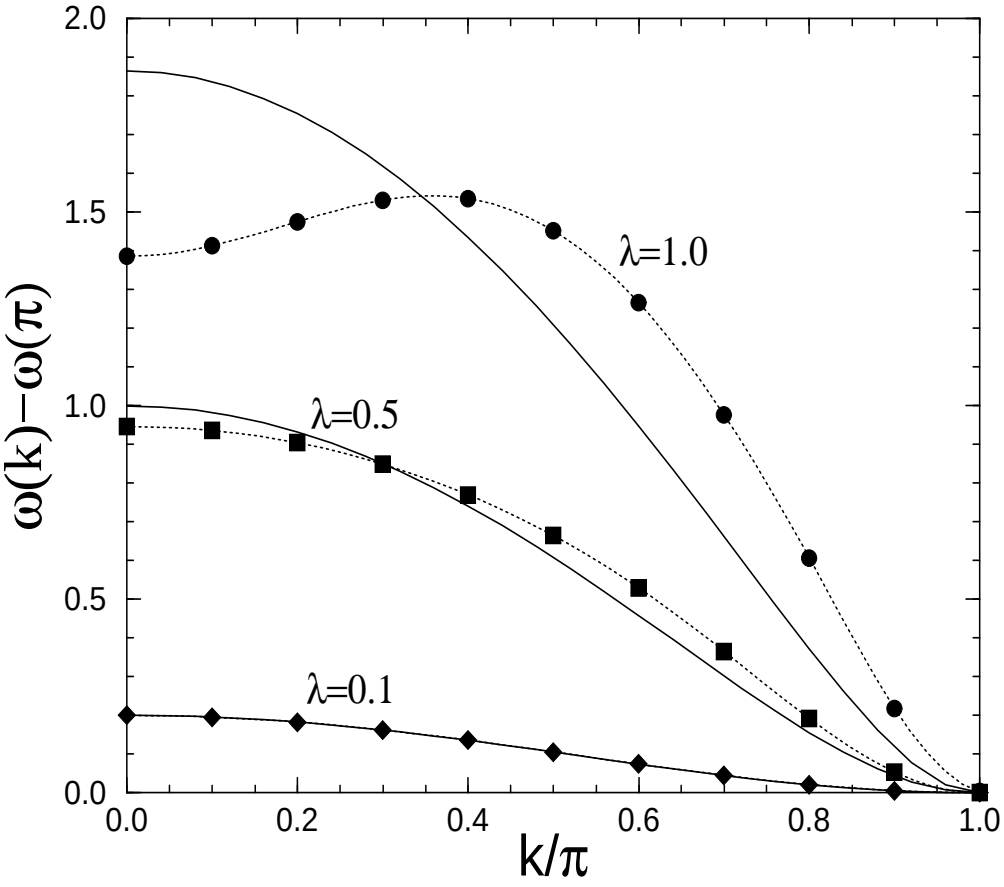

FIG. 3. Spin-triplet dispersion band relative to the band minimum (in units of $J_\perp$) as a function of momentum. The filled symbols are exact results [8,13] (see text); the dotted lines joining them were obtained from a cubic-spline fit.

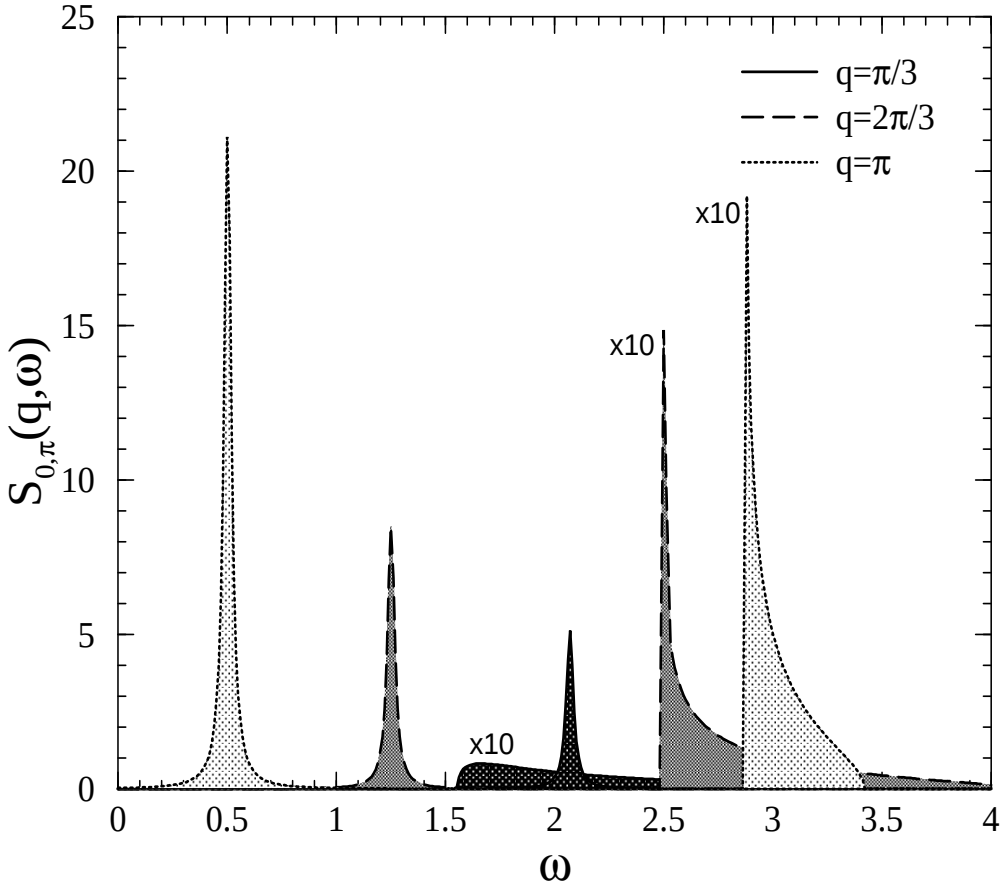

FIG. 4. Dynamic spin responses S_0 and S_π in the rung basis as a function of ω for various values of q. The responses were computed at the isotropic value of $\lambda = 1$. All S_0 responses have been multiplied by a factor of 10, while the S_π responses include a smearing factor of 0.02.

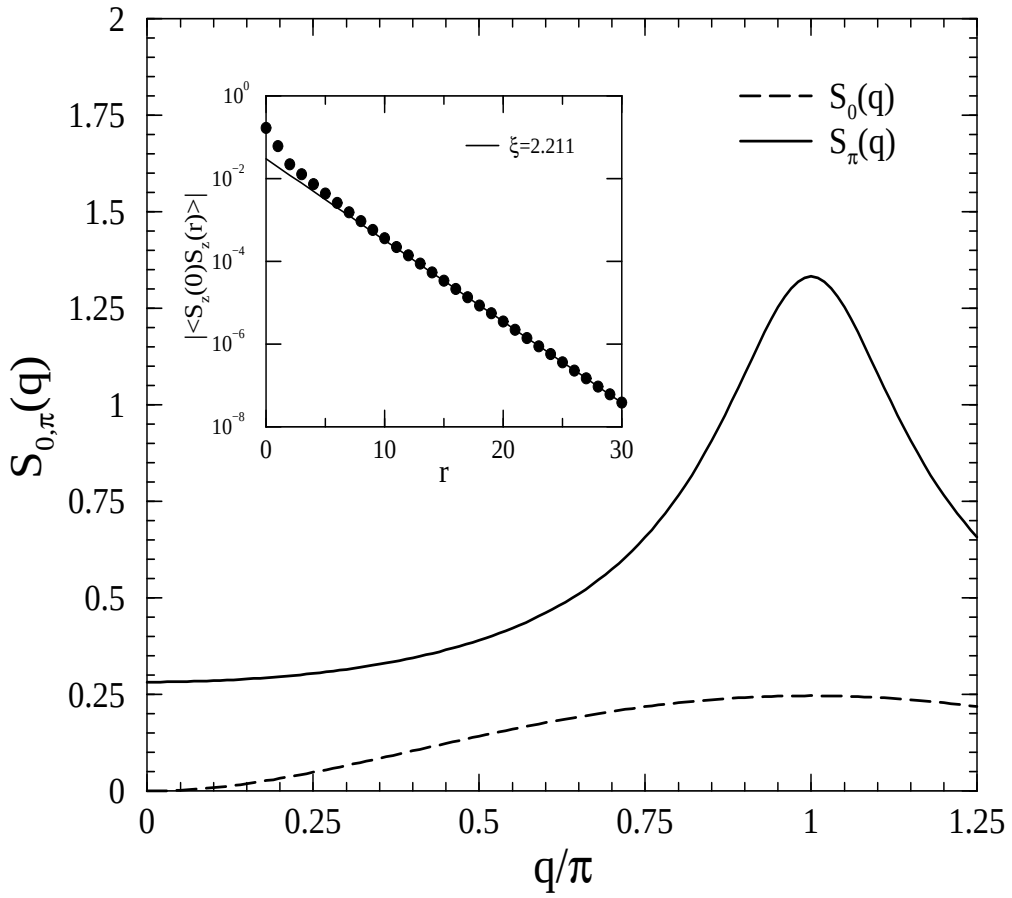

FIG. 5. Static structure factors S_0 and S_π in the rung basis as a function of q for $\lambda = 1$. The inset shows a logarithmic plot of the spin-spin correlation as a function of r. A value of $\xi = 2.211$ is obtained for the spin-spin correlation length from the slope of the straight-line fit.

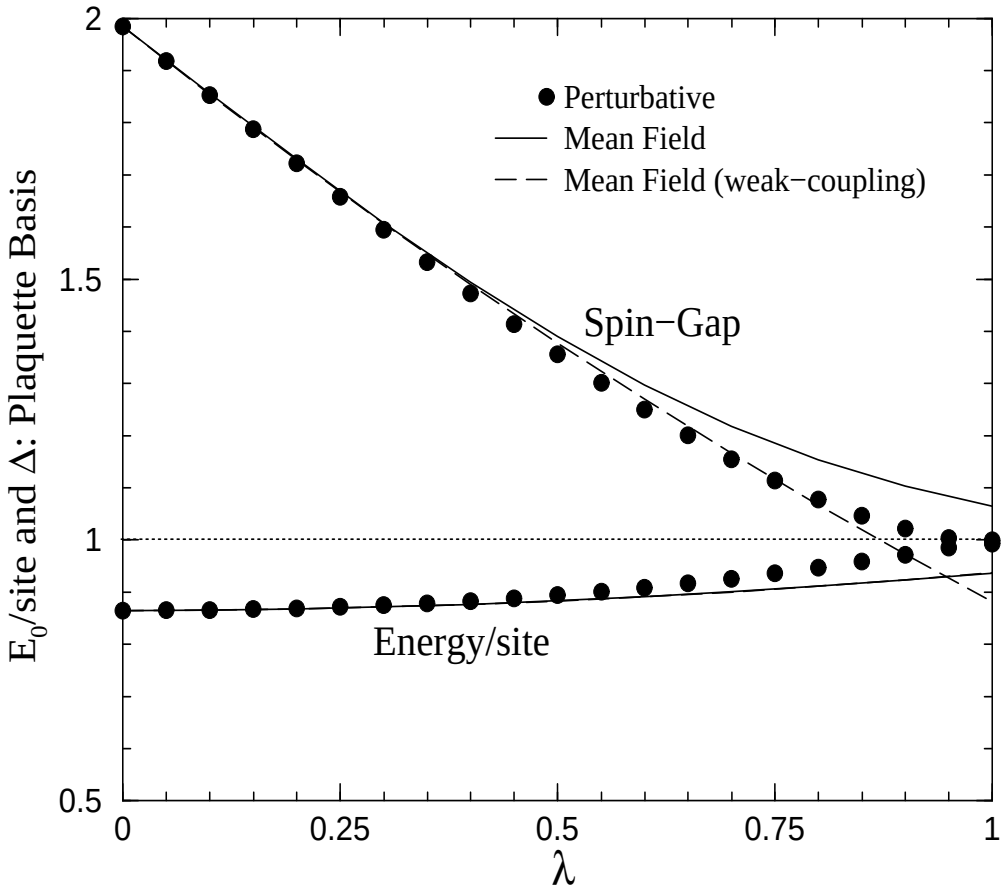

FIG. 6. Energy-per-site and singlet-triplet gap as a function of λ in the plaquette basis. Quantities plotted are ratios to their exact values at the isotropic ($\lambda = 1$) point. The filled circles are from high-order perturbative calculations [8].

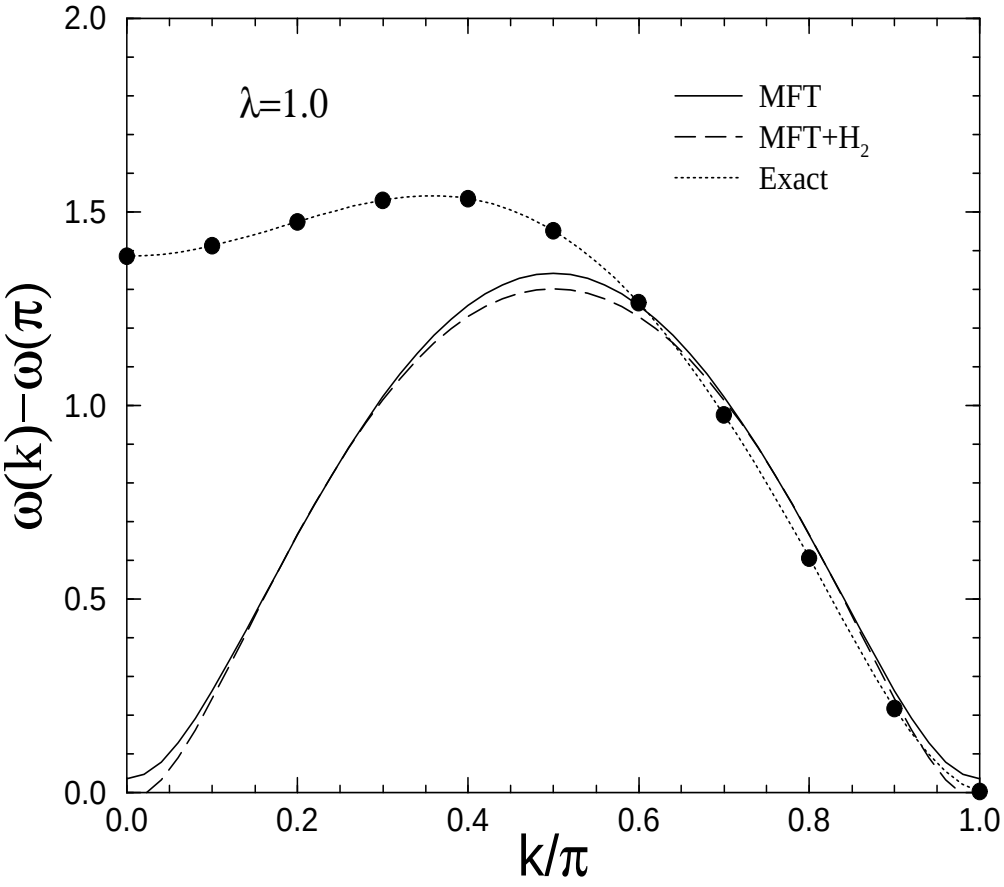

FIG. 7. Spin-triplet dispersion band relative to the band minimum in the plaquette basis as a function of momentum. The filled symbols represent exact results [13].

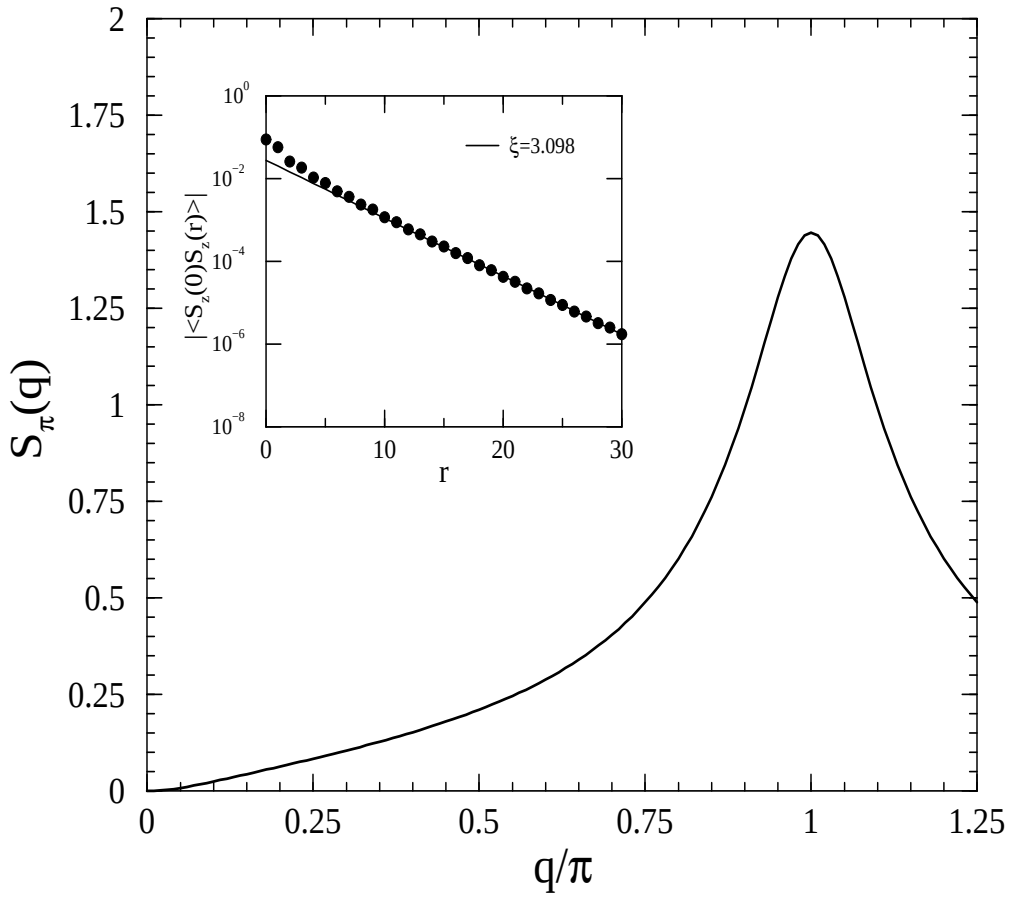

FIG. 8. Static structure factors S_π in the plaquette basis as a function of q at the isotropic point; the structure factor S_0 vanishes in the (low-energy) plaquette basis. The inset shows a logarithmic plot of its Fourier transform; the indicated straight-line fit yields a value of $\xi = 3.098$ for the spin-spin correlation length.

TABLES

TABLE I. Unperturbed singlet/triplet energies and the two independent matrix elements in various angular-momentum-coupled bases.

Basis	ϵ_0	ϵ_1	$\alpha \equiv \langle 011 \| \| V(1,2) \| \| 101 \rangle$	$\beta \equiv \langle 110 \| \| V(1,2) \| \| 110 \rangle$
2×1	$-3/4$	$+1/4$	$+1/2$	-1
2×2	-2	-1	$-1/3$	$-1/4$
2×4	-4.29307	-3.52286	-0.20805	-0.08625

TABLE II. Results for the ground-state energy-per-site and for the singlet-triplet gap (displayed inside brackets) for a few values of λ in the Rung basis.

λ	Ref. [7]	Present work	Exact
0.25	-0.37908 [0.72846]	-0.38683 [0.76699]	-0.38804 [0.78438]
0.50	-0.39392 [0.40411]	-0.42237 [0.59685]	-0.42911 [0.64065]
1.00	-0.47531 [0.10291]	-0.54285 [0.50133]	-0.57804 [0.50400]

TABLE III. Results for the ground-state energy-per-site and for the singlet-triplet gap (displayed inside brackets) for various angular-momentum coupled bases. Listed are zeroth-order, mean-field, mean-field plus H_2, and exact results (see text for details). The exact values were extracted from DMRG calculations. The last column lists the spin-singlet condensate fraction.

Basis	Zeroth-order	MFT	MFT+H_2	Exact	$\bar{s}^2$
2×1	-0.37500 [1.00000]	-0.54285 [0.50133]	-0.58849 [0.13204]	-0.57804 [0.50400]	0.78129
2×2	-0.50000 [1.00000]	-0.54112 [0.53689]	-0.54498 [0.48154]	-0.57804 [0.50400]	0.85826
2×4	-0.53663 [0.77021]	-0.54724 [0.44566]	-0.54774 [0.43216]	-0.57804 [0.50400]	0.89628

TABLE IV. Results for spin spin-spin correlation lengths for the rung and plaquette bases. The "Fit" results are obtained by straight-line fits to semi-log plots of the correlation function as determined by numerical evaluation of the integral appearing in Eqn.(37). The "Analytic" results are obtained using Eqns.(53) and (58) for rung and plaquette bases, respectively. The "Exact" value is from the DMRG calculation of Ref. [3].

Basis	Fit	Analytic	Exact
2×1	2.211	2.323	3.19
2×2	3.098	3.327	3.19